Volume 16, No 4 | International Journal of Radiation Research, October 2018

A feasibility study of dynamic verification for tumor target delineation and dose delivery using a six degrees of freedom motion phantom

G. Xu[1,2,3], Z. Xiong[4], H. Wang[3], H. Jiang[2,5,6*], B. Li[3], L. Liu[3]

[1]University of Chinese Academy of Sciences, Beijing 100049, China
[2]Center of Medical Physics and Technology, Hefei Institutes of Physical Science, Chinese Academy of Sciences, Hefei 230031, China
[3]Cancer Hospital, Hefei Institutes of Physical Science, Chinese Academy of Sciences, Hefei 230031, China
[4]Department of Physiology and Biophysics, State University of New York at Buffalo, Buffalo, NY, USA
[5]Anhui Institute of Optics and Fine Mechanics, Chinese Academy of Sciences, Hefei 230031, China
[6]Department of Optics and Optical Engineering, University of Science and Technology of China, Hefei 230026, China

► ***Original article***

Corresponding authors:
Dr. Haihe Jiang,
Fax: *+86 0551 65591667*
E-mail:
Email: hjiang@aiofm.ac.cn

Revised: September 2017
Accepted: October 2017

Int. J. Radiat. Res., October 2018; 16(4): 411-420

DOI: 10.18869/acadpub.ijrr.16.4.410

ABSTRACT

Background: The dynamic phantom is one of the best tools to study the impact of motion on tumor target delineation and absorbed dose verification during dose delivery. ***Materials and Methods***: this study, a 6-DOF (degrees of freedom) phantom was designed following the stacked serial kinematics and assembled by six commercial motion stages to generate 6-DOF motion, which were RotX (pitch, around X), RotY (roll, around Y), TransZ (anterior–posterior), RotZ (yaw, around Z), TransY (superior–inferior) and TransX (left–right). Tumor targets were designed by six plastic spheres for the delineation test. Also, an ionization chamber array detector and RW3 solid water were combined to measure the absorbed dose for dose verification tests. ***Results:*** The maximum translation speeds for LineX and LineY were 50mm/s and 35mm/s for LineZ, while the maximum rotation speeds for RotX, RotY, RotZ were 5.33° per second, 6° per second and 15° per second respectively. Spiral-CT and 4D-CT images acquired in the static and dynamic states successfully showed the influences of tumor motion on target delineation. In the absorbed dose verification, all cases did not pass the gamma test; the pass rate for the 6-DOF motion case was only 34.2% and the pass rates of all other cases were less than 90%. ***Conclusion:*** The phantom designed in this study is able to simulate complex tumor motion and can be used to study the influence of tumor motion in radiotherapy.

Keywords: *6DOF dynamic phantom, respiratory motion, image artifacts, dose verification, external marker tracking.*

INTRODUCTION

Respiration-induced motion presents a significant challenge for treating thoracic and abdominal tumors. Motion can degrade image quality, which makes it hard to delineate the target margins and interferes with the delivery of the desired dose distribution [1]. In order to quantify the impact of motion on radiotherapy, many in-house created phantoms have been constructed. For example, in early research, with the help of a 1-DOF motion phantom, Keall [2] demonstrated the feasibility of motion adaptive x-ray therapy and evaluated the capabilities of the treatment machines to deliver such treatments. More complex motion types have been reported [3-5], and Hsieh [6], Nakayama [7], Bandala [8], and Grohmann [9] reported the designs and applications of four types of 3-DOF linear motion phantoms with independent

[Downloaded from ijrr.com on 2026-11-24]

motion along any X, Y, and Z direction. Haas [10] developed a thorax phantom with independent rib cage and tumor motion. Using a robotic arm and a commercial artificial skeleton, Steidl [11] designed a phantom to realize 1-DOF rib cage motion and 6-DOF tumor motion, which included 3-DOF linear motion and 3-DOF rotation along pitch, roll and yaw. Following the Stewart–Gough parallel kinematics, Belcher [12] built a 6DOF phantom to simulate tumor motion. Reports also revealed that 6-DOF treatment couches like HexPOD (Elekta, Co., Ltd., Stockholm, Sweden) and TrueBeam (Varian, Inc., Palo Alto, Canada) can also be used as a phantom to simulate tumor motion in 6-DOF [13,14]. However, the 6-DOF treatment couch can't be used for CT scanning. Additionally, the study of robotic arm phantom and the Stewart–Gough phantom did not show the ability of loading ionization chamber array detector for dose verification. In order to investigate the motion impacts mentioned above, the requirements for a 6-DOF prototype phantom can be summarized as the following properties:

a) The phantom could be used to simulate single direction motion and synchronized motion. (e.g. synchronized 6DOF motion).
b) The 4DCT scanner can be used to obtain a phantom image in a static or dynamic state.
c) A unique solution for motion or a motion sequence does not affect the final position of the phantom. For example, the tumor may stop at a different position while rotating at the same angle but with a different sequence, and the result is not unique.
d) The phantom must have the ability to hold quality assurance (QA) detectors, e.g. MatriXX (IBA, Co., Ltd., New Leuven, Belgium), OCTIVUS (PTW, Co., Ltd., Freiburg, Germany), and water-equivalent slabs, e.g. RW3 slices (PTW, Co., Ltd., Freiburg, Germany).

In order to meet the needs of this study, stacked serial kinematics with independent motion along any X, Y, Z, pitch, roll, and yaw axis has been used to develop the 6-DOF phantom prototype. The phantom characteristics and its first feasibility application in CT-image reconstruction and in dynamic dose verification tests have been discussed below.

MATERIALS AND METHODS

Technical specifications of the phantom

Considering the above four aspects, six independent commercial motion stages are assembled to generate 6-DOF motion, as shown in figure 1 (a) and (b). RotX and RotY parts were composed of a two ball bearing arc slider (SA10A-RT, STAGE KOHZU, Co., Ltd., Kanagawa, Japan) while RotZ is a modified rotation stage (KST-YAW, SIGMA KOKICO, Co., Ltd., Tokyo, Japan). LineZ is a lifting platform (OSMS-ZF, SIGMA KOKICO, Co., Ltd., Tokyo, Japan), while LineX and LineY were horizontal sliders (Parker Hannifin Motion & Control Co, Ltd., Kaarst, Germany). In addition, in order to simulate the respiration signal by driving the signal strip of the 4D-CT scanner, an independent linear screw with a 42-stepper motor was used. The 42-stepper motor driver was connected to the motion phantom to obtain the same motion trajectory. The IR (infrared) calibration tool for HexPOD, as shown in figure 1(a), is placed on the top of the motion phantom. The IR monitor (Polaris Spectra, Northern Digital Inc., Ontario, Canada) can be used to record the trajectory of the motion phantom. The motion control system consists of two-stepper motor controllers (MC-XYZ, BENT-CN, Co., Ltd., Zhejiang, China) and six-stepper motor drivers (TB6600, YIXING Technology, Co., Ltd., Jiangsu, China).

For tumor target delineation test, six plastic spheres were used to simulate the tumor target as shown in figure 1(a). The largest sphere, of which the diameter is 40mm, is set in the center to simulate the main tumor shape, while the five small spheres, of which diameter is 20mm, are used to simulate the tumor branches. The design is aimed to test how the motion patterns affect the tumor margin delineation.

For dose verification test, water-equivalent slabs (RW3, PTW, Co., Ltd., Freiburg, Germany) as shown in figure 1 (b), were loaded on the top of the phantom. The ionization chamber array (OCTAVIUS® 729, PTW, Co., Ltd., Freiburg, Germany) is adopted as the detector and inserted into the middle of the RW3 slabs. The number of water-equivalent slabs can be changed based on the needs of specific

[Downloaded from ijrr.com on 2026-11-24]

experiments, but less than the maximum working load. Because of the height of the phantom, the gantry of the LINAC could not rotate a whole circle around the phantom during dose delivery. This limitation will be discussed below.

Evaluation phantom positioning accuracy

The IR camera, which was used to monitor the HexPOD treatment couch, was adopted to monitor the phantom motion in this study. The calibration tool with six infrared ray reflecting balls was used to calibrate the 6DOF treatment couch as shown in figure 2(a). In this study it was adopted to determine the positioning accuracy of the 6DOF motion phantom. The infrared ray camera can record the position of the balls, labeled as A, B, C, D, and E, in the camera coordinate system as shown in figure 2 (a). Before using the calibration tool, a position model file, as shown in figure 2(b), should be made under the calibration tool coordinate system using the 6D Architect software (Polaris Spectra, Northern Digital Inc., Ontario, Canada). The location of the five IR reflector spheres on the calibration tool can be recorded and displayed via the tracking mode in the Tool Box software (Polaris Spectra, Northern Digital Inc., Ontario, Canada). As the coordinate transformation equation has been embedded in the 6D Architect software, trajectories calculation could be avoided and the original position of the IR reflection sphere can be transformed to the camera coordinate. For example, in order to avoid comparing the rotation angles by degree unit, the comparison of points C, D, and E can be made by mm unit between the position recorded by the monitor and the position calculated by the software to check the accuracy of the phantom motion. This simple method can avoid programming to realize complex trajectory calculation algorithm.

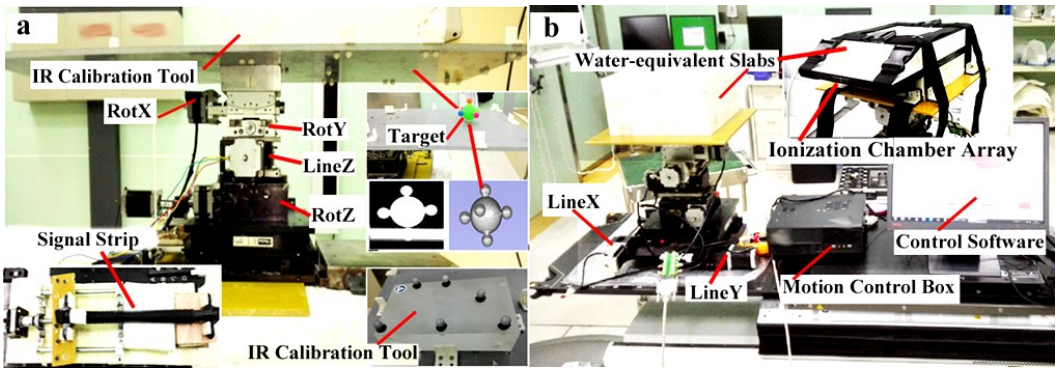


Figure 1. The 6DOF motion phantom. In this figure, figure labeled **(a)** represents the 6DOF phantom applied in target delineation and figure labeled **(b)** represents the6DOF phantom applied in dose verification. LineX, LineY and LineZ represent the stages which could generate translations along X, Y, Z axes respectively, while RotX, RotY and RotZ mean the stages which could generate rotations around X, Y, Z axes respectively.

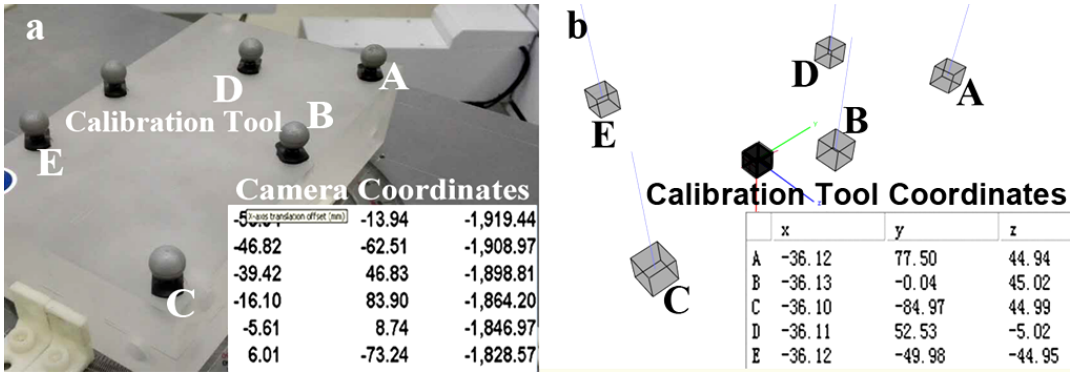


Figure 2. Calibration tools in different coordinates. In this figure, figure labeled **(a)** represents the original transform from calibration tool coordinates to IR camera coordinates and figure labeled **(b)** represents the Original position of IR reflection points in the 6D Architect software.

[Downloaded from ijrr.com on 2026-11-24]

Feasibility in image acquisition and dynamic dose verification

To investigate the impacts of motion on image acquisition and reconstruction during spiral-CT and 4D-CT scanning, the phantom movement was arranged in ten different motion patterns, static, six single DOF motions, 3-DOF translation, 3-DOF rotation and 6-DOF movement. In this study, the maximum motion ranges were set to 10 mm, 15 mm, 6 mm, 1.9°, 3°, 2.4° for TransX, TransY, TransZ, RotX, RotY and RotZ respectively, due to rotation-induced translation and linear motion platform compensation.

And for the feasibility test of dynamic dose verification, a VMAT (Volumetric-Modulated Arc Therapy) plan for thorax tumor was calculated on this 6-DOF phantom in the QA mode of MONACO software (Elekta, Co., Ltd., Stockholm, Sweden). Due to the height of this phantom, the gantry was set to rotate just around the top of the phantom to avoid radiating the metal components. During the dose delivery by the Axesse LINAC (Elekta, Co., Ltd., Stockholm, Sweden), the phantom movement was also arranged in the ten patterns as described above. The absorbed dose measured in a dynamic state was then compared to a static state with the help of the Verisoft (PTW, USA). The pass rates were analyzed by γ-Test and the criteria was 90%, which is used as a common standard in radiotherapy. In addition, physicists usually examine the cold and hot points to assess a radiotherapy plan, and this evaluation methodology was also brought in this feasibility study. The cold point means the dose of dynamic states are smaller than that of the static state, while the hot point means the dose of dynamic cases are larger than that of the static state. All the cold and hot points are failed to pass the γ-Test. All the results were divided into two groups, i.e. the Up5% and Up30%. In the Up5% group, the points, of which the doses were smaller than 5% of the max dose, didn't be evaluated, while in the Up30% group, we only evaluated the points of which the doses were smaller than 30% of the max dose.

RESULTS

Basic characteristics

The movement speed varies with the capacity of each stage, faster the stepper motor rotates, smaller the motor power is. Therefore, take the RotX slider for instance, as shown in figure 3, the velocity curve is fitted by Matlab software. In this test, the maximum translation speed for LineX and LineY was 50 mm/s and 35 mm/s for LineZ, while the maximum rotation speed for RotX, RotY, RotZ was 5.33° per second, 6° per second and 15° per second respectively. The basic characteristic comparison of the typical 6-DOF phantoms are shown as table 1.

For translation tests, the motion distances were selected to 2 mm, 5 mm, 10 mm, and 20 mm to evaluate the positioning accuracy, while for rotation tests, 1°, 2°, 5°and 6 °angles were chosen to assess the rotation accuracy. In order to test the repeat positioning accuracy in each direction, the peak-to-peak motion at a frequency of 20 times per minute was selected to repeat the above range. The average error of all translations did not exceed ± 0.2 mm, and the average error of all rotations did not exceed ± 0.3 mm, as shown in table 2. The maximum translation error for LineZ was -0.54 mm, and the maximum rotation error for RotZ was -0.82 mm. The maximum error for 6-DOF motion was -0.79 mm, and the average error of it did not exceed ± 0.1 mm.

Tumor target delineation

CT slice thickness was set to 3 mm before scanning, and ten-phase mode was adopted for 4D-CT scanning. After scanning, the spiral CT images were compared with 50% phase 4D-CT images with the same motion patterns. The CT volume was reconstructed by 3D slice software, as shown in figure 4. The deformation occurs on all spiral-CT images which are acquired in dynamic state, while the shape changes slightly for the 4D-CT images. For the motions of LineX, LineY, LineZ, RotX, and RotY stages, the main spheres structure can be characterized easily, especially for the motion of RotY stage where the

[Downloaded from ijrr.com on 2026-11-24]

structure is almost unchanged. However, for the motion of RotZ stage, 3-DOF rotation, 3-DOF translation and the 6-DOF motion, the structural changes can be clearly distinguished, and some structural information misses in superior–inferior direction, while the some structural information adds in the left-right direction. The tumor branch spheres also show significant changes depending on the motion patterns, and there is a clear lack of information in the motion type with a rotation around the Z direction. For all translations without rotation, the structure changes. Although the deviations of the center sphere and the small sphere don't appear, these deviations appear in all the rotations of the movement. For the LineX and LineY motion tests, the center sphere structure was compressed along the direction of motion. However, this phenomenon did not appear significantly in the LineZ motion test. In the RotZ motion test, the information of the front small sphere is lost in both the spiral-CT and 4D-CT images. Additionally, two artifacts appeared around the top sphere.

Dynamic dose verification

The γ-Test results for the respiratory rate of 20 per minute are shown in table 2. The results of all motion patterns did not pass the γ-Test, i.e. all the results were smaller than 90%. Take the Up5% group for example, in the cases of single DOF motions, LineZ translation and RotX rotation had the highest pass rates, 79.8% and 77% respectively. Then, pass rates of LineX and RotZ are 70.1% and 68.8%, respectively. The LineY and RotY had the lowest pass rate, which were 34.4 % and 56.3%, respectively. The 3-DOF translation had a pass rate of 39.1%, which was greater than the rate of LineY movement, but significantly less than the rate of LineX and LineZ movement. The 3-DOF rotation had a pass rate of 52.8%, which was less than all the single direction rotations, but greater than the pass rate of 3-DOF translation movement. For integrated 6-DOF motion, the pass rate was 34.2%, which was the lowest of all the motion patterns. In the cases of the Up30% group, the similar trend can be observed from the table 2.

For LineY, RotY and 6-DOF cases, the γ-Test images are shown in figure 5 and the failed points of each motion patterns are shown in figure 6. In these figures, most of the dose divergence is located outside the target area and the edge of the target, which is also a sharp dose gradient region. The results reveal that there is almost no transition between the passing area and the failed area. For the LineY motion, significant dose divergence occurs in the superior–inferior and left-right direction, but in the RotY motion test, the divergence is mainly in the left-right direction. In the two types of tests, there are some hot points higher than the planned dose at the side of motion ending, while the cold points below the planned dose appear mainly on the beginning of the motion. In the case of 6-DOF movement, much more hot and cold points appear, and they are distributed diagonally.

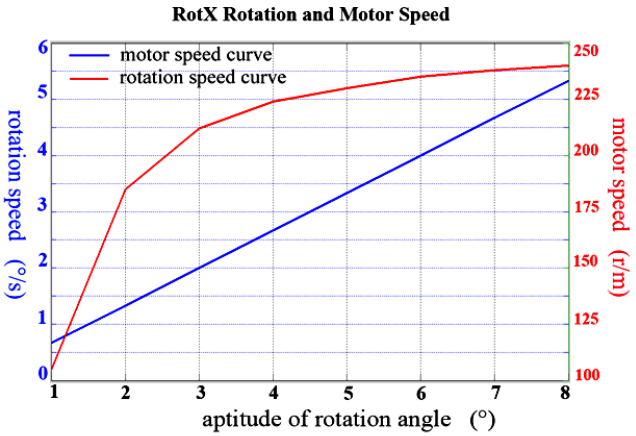


Figure 3. RotX stage motion and motor speed curve with 20 times per minute frequency.

[Downloaded from ijrr.com on 2026-11-24]

Table1. Basic Characters Comparison

Study	Load (kg)	Max Speed [a]						Max Range [b]					
		LineX	LineY	LineZ	RotX	RotY	RotZ	LineX	LineY	LineZ	RotX	RotY	RotZ
HexPod[13]	~200	16	16	16	—	—	—	60	60	80	6	6	6
TrueBeam couch[14]	200	—	—	—	—	—	—	80	80	80	6	6	6
Belcher [12]	32	40.7	38.1	18.8	17.4	18.1	44.6	84.4	90.9	31.1	29	30	82
This study [c]	20	50	50	35	5.3	6	15	150	150	20	10	10	30

a. For translations, mm/s and for rotations, °/s.
b. For translations, mm and for rotations, °.
c. In this study, LineX, LineY and LineZ represent the translations along X, Y, Z axes respectively, while RotX, RotY and RotZ mean the rotations around X, Y, Z axes respectively. For further illustration, a video attachment can be found online (available from https://pan.baidu.com/s/1c2ktSOS) showing the motion of the phantom.

Table 2. Results of Phantom Accuracy and Absorbed Dose γ-Test

Motion [a]	Repeating Accuracy(mm)				Failed Points/ Evaluated points		Max Difference (Gy)	γ-Test Result	
	Min Error	Max Error	Mean ± SE	RSME[b]	Up5%[c]	Up30%[d]		Up5%[c]	Up30%[d]
LineX	0.01	0.47	0.13 ± 0.0368	0.1899	100/334	58/135	0.545	70.1%	50.7%
LineY	0.01	-0.54	-0.10 ± 0.0682	0.2756	225/343	70/138	0.951	34.4%	49.3%
LineZ	0.01	-0.35	-0.006 ± 0.0388	0.1452	68/337	16/139	0.127	79.8%	88.5%
RotX	0.12	0.82	0.01 ± 0.1076	0.4029	77/335	19/141	0.230	77%	86.5%
RotY	0.01	-0.52	-0.09 ± 0.0636	0.2560	147/336	23/138	0.282	56.3%	83.3%
RotZ	-0.02	-0.59	-0.11 ± 0.0817	0.3250	135/336	27/133	0.274	68.8%	79.7%
3DOF Translation	-0.01	0.69	0.17 ± 0.0608	0.2821	212/348	63/140	1.034	39.1%	55.0%
3DOF Rotation	-0.03	0.45	0.20 ± 0.0329	0.2388	159/337	34/131	0.912	52.8%	74.0%
6DOF Motion	-0.12	-0.79	-0.05 ± 0.1088	0.4104	227/345	79/142	1.094	34.2%	44.4%

a. In this study, LineX, LineY and LineZ represent the translations along X, Y, Z axes respectively, while RotX, RotY and RotZ mean the rotations around X, Y, Z axes respectively. The 3DOF Translation represents the combination of the LineX, LineY and LineZ translations, and the 3DOF Rotation is the combination of the RotX, RotY and RotZ rotations. The 6DOF Motion represents the combination of all the three patterns translations and three patterns rotations.
b. RMSE represents root mean square error.
c. The title, Up5%, represents that the dose of the evaluated points were larger than the 5% of the max dose.
d. The title, Up30%, represents that the dose of the evaluated points were larger than the 30% of the max dose.

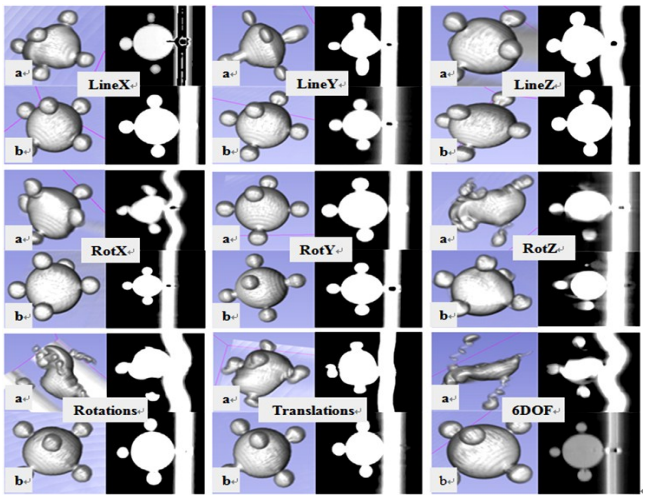


Figure 4. CT reconstruction results. The (a)-figures and (b)-figures represent CT-imaging and reconstruction while the phantom is moving. The images labeled a represent the result of a spiral CT reconstruction, and the images labeled b indicate the result of the 4DCT reconstruction based on the fifth phase CT set. In this feasibility study, all the CT sets were reconstructed by 3D Slicer software. LineX, LineY and LineZ represent the translations along X, Y, Z axes respectively, while RotX, RotY and RotZ mean the rotations around X, Y, Z axes respectively. The Translation represents the combination of the LineX, LineY and LineZ translations, and the Rotations is the combination of the RotX, RotY and RotZ rotations. The 6DOF Motion represents the combination of all the three patterns translations and three patterns rotations.

[Downloaded from ijrr.com on 2026-11-24]

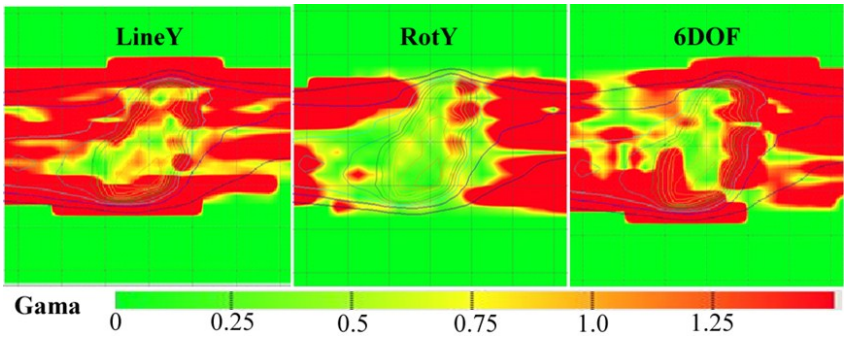


Figure 5. The γ-Test result for LineY, RotY and 6DOF motion. LineY and RotY represent the translations along and rotations around Y axis respectively, while the 6DOF represents the combination of all the three patterns translations and three patterns rotations. If the gamma value is larger than 1, this point is failed to pass theγ-Test.

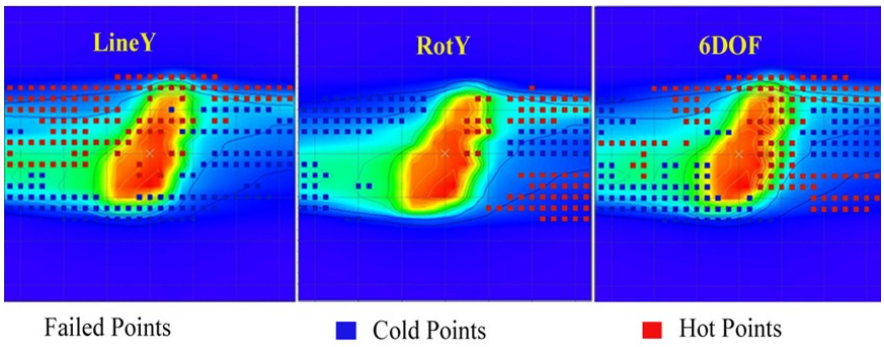


Figure 6. The failed points result of LineY, RotY and 6DOF motion. LineY and RotY represent the translations along and rotations around Y axis respectively, while the 6DOF represents the combination of all the three patterns translations and three patterns rotations. The cold point means the dose of dynamic states are smaller than that of the static state, while the hot point means the dose of dynamic cases are larger than that of the static state.

DISCUSSION

Phantom performance and limits

The dynamic phantom is a very important tool for investigating the dynamic affects during the entire radiotherapy process and it can also be used as a validation benchmark to test the performance of the radiotherapy program software, especially for the four-dimensional dose calculation system [15, 16]. Steidl [11] defines nine basic characteristics of the phantom which were applied in ion beam therapy and these characteristics are also suitable for photon beam therapy. However, the most important functions are imaging and dose validation. As Tlusty [17] and Kurekova [18] reported, Stacking and parallel motions have their own advantages and disadvantages, and comparing the robotic arm and the Stewart-Gough phantom model. The 6-DOF phantom model designed in this study has a unique position model, i.e. the rotation or translational motion sequence can't affect the final location of the phantom, which makes it easy to program the motion control code.

The maximum motion aptitudes, which were 150 mm for LineX and LineY, 20 mm for LineZ, 10° for RotX, 10° for RotY, and 30° for RotZ, could generally cover the reported motion ranges [5]. When assembling this phantom, several commercial sliders were used. The phantom size used in this study is 35 cm in height and not suitable for whole circle VMAT or arc radiotherapy test. In the next design, the phantom height will be reduced, and the LineX and LineY sliders will be replaced by a in-house made slider. In this prototype phantom, 57-stepper motors were used to drive the dynamic stages. Due to the power limit, the maximum load of this phantom was 20kg which was sufficient to meet our needs. In the future, a more powerful servo motor will be used and will make the structure more compact to reduce

[Downloaded from ijrr.com on 2026-11-24]

wobble during movement and gain more load capacity.

Feasibility in clinical usage

CT images acquiring is the first step in the radiotherapy process, and all photon radiotherapy is based on CT images to obtain tumor target margins. But the tumor movement produces artifacts in the CT images which significantly affect the delineation work and cause a serious dose error in the radiotherapy plan. This study shows the feasibility for studying these affects with the help of this 6-DOF dynamic phantom. As figure 4 reveals, different deformations can be gotten by CT images scanned under different motion patterns generated by this phantom. Ford [19], Keall [20], D'Souza [21], Fitzpatrick [22] and Suh [23], investigated the method of measuring the respiratory-induced anatomic motion by an eccentric wheel driven phantom, but the patterns of motion were simple. The 6-DOF phantom exhibited high performance in generating multiple DOF motions, and similar studies with the aid of this phantom will be reported step by step.

Another purpose of designing this 6-DOF dynamic phantom was to verify motion-induced dose divergence during dose delivery with the LINAC. As shown in table 2, there was no normalized dose pass rate higher than 95%, which was very similar to what Steidl [11], Richter [24], Menon [25] and Court [26] reported in their studies. In this study, in order to avoid the uncertainty of the detector, points for which the normalized rate greater than 30% of the ISO center dose were also chosen to be analyzed by γ-Test method, but the pass rate was still less than 95%, which is a common QA standard in the clinic. About 70% to 80% of the failure regions or failure points appeared outside the target, and these areas and points were located in the areas of the normal tissues. But this does not mean that the motion did not affect the target area. Especially in the LineY, 3-DOF translation, 3-DOF rotation and 6-DOF motion test cases, a volume of failed areas and points appeared inside the target area. Qualitatively, the cold points always appeared in the beginning of the movement, in the mean while hot points always appeared at the end of the motions. Our study recommended to pay much more attention to the tumor target rotations, as the impact of these movements was no less than the effect of translation on the absorbed dose. One clinical plan has been tested to test the feasibility of this phantom and more clinical cases will be examined in the future to make validation and analysis more reasonable.

In this feasibility study, the results of tumor target shape change and dose divergence showed a high positive correlation. The 6-DOF motion type resulted in the largest shape change and dose divergence. LineZ motion type induced the smallest dose divergence, although the shape change was the second smallest. In the RotY motion test, the shape change was minimal and the dose pass rate is also very high. The pass rates of single DOF motions were usually better than those of multiple DOF motions, and the pass rates of unidirectional translations were usually better than those of unidirectional rotation. In this study, the pass rates of motion along and around Y direction were at a low level.

CONCLUSION

In this study, a 6-DOF dynamic phantom was successfully developed to assess the effect of target motions on tumor target delineation and dose verification. The basic phantom characteristics fitted our research needs and the feasibility tests showed that the phantom successfully produced different motion patterns that could induce tumor targets deformation and absorbed dose divergences. This study also provides an easy way to use existing equipment such as ionization chamber array detector and water-equivalent slabs, which are frequently used as clinical QA tools, to realize a complex dynamic verification procedure. In the future, improvements will be added to this phantom and more test cases will be checked to find the approaches to minimize the image artifacts and dose divergences caused by target motion in the radiotherapy procedure.

[Downloaded from ijrr.com on 2026-11-24]

ACKNOWLEDGMENTS

This work was funded in part by the Spark Research Grant from the CMPT (Center of Medical Physics and Technology, Hefei Institutes of Physical Science, CAS). The authors would also like to thank, Professor Hai Li, Dr. Jin Jing and all the fellows of the Radiotherapy Center, CMPT for their help during this study.

Conflicts of interest*: *Declared none.

REFERENCES

1. Kissick, Michael, and T. Mccaw (2014) Motion Phantoms for Radiotherapy. In: The Phantoms of Medical and Health Physics. Springer New York, USA.
2. Keall PJ, Kini VR, Vedam SS, Mohan R (2001) Motion adaptive x-ray therapy: a feasibility study. *Phys Med Biol, **46**: 1-10*.
3. Seppenwoolde Y, Shirato H, Kitamura K, Shimizu S, van Herk M, Lebesque JV, Miyasaka K (2002) Precise and real-time measurement of 3D tumor motion in lung due to breathing and heartbeat, measured during radiotherapy. *Int J Radiat Oncol, **53**: 822-834*.
4. Plathow C, Schoebinger M, Fink C, Hof H, Debus J, Meinzer H-P, Kauczor, H-U (2006) Quantification of lung tumor volume and rotation at 3D dynamic parallel MR imaging with view sharing: preliminary results. *Radiology, **240**: 537-545*.
5. Huang CY, Tehrani JN, Ng JA, Booth J, Keall P (2015) Six degrees-of-freedom prostate and lung tumor motion measurements using kilovoltage intrafraction monitoring. *Int J Radiat Oncol Biol Phys, **91**: 368-375*.
6. Malinowski K, Lu W, Lechleiter K, Low D, Parikh P (2007) Development of the 4D Phantom for patient-specific end-to-end radiation therapy QA. *SPIE, **6510**: 65100E-65100E-9*.
7. Nakayama H, Mizowaki T, Narita Y, Kawada N, Takahashi K, Mihara K, Hiraoka M (2008) Development of a three-dimensionally movable phantom system for dosimetric verifications. *Med Phys, **35**: 1643-1650*.
8. Bandala M and Joyce MJ (2013) A Computer-Controlled Dynamic Phantom for Respiratory-Gated Medical Radiotherapy Research. *IEICE T Fund Electr, **E96.A**: 1609-1616*.
9. Grohmann C, Frenzel T, Werner R, Cremers F (2014) Design, performance characteristics and application examples of a new 4d motion platform. *Z Med Phys, **25**: 156-167*.
10. Haas OC, Mills JA, Land I, Mulholl P, Menary P, Crichton R, Depuydt T (2014) IGRT/ART phantom with programmable independent rib cage and tumor motion. *Med Phys, **41**: 022106-1-022106-6*.
11. Steidl P, Richter D, Schuy C, Schubert E, Haberer T, Durante M, Bert C (2012) A breathing thorax phantom with independently programmable 6D tumour motion for dosimetric measurements in radiation therapy. *Phys Med Biol, **57**: 2235-2250*.
12. Belcher AH, Liu X, Grelewicz Z, Pearson E, Wiersma RD (2014) Development of a 6dof robotic motion phantom for radiation therapy. *Med Phys, **41**: 121704-1-121704-7*.
13. Menten MJ, Guckenberger M, Herrmann C, Krauss A, Nill S, Oelfke U, Wilbert J (2012) Comparison of a multileaf collimator tracking system and a robotic treatment couch tracking system for organ motion compensation during radiotherapy. *Med Phys, **39**: 7032-7041*.
14. Sweeney RA, Arnold W, Steixner E, Nevinny-Stickel M, Lukas P (2009) Compensating for tumor motion by a 6-degree-of-freedom treatment couch: is patient tolerance an issue? *Int J Radiat Oncol Biol Phys, **74**: 168-171*.
15. Chan MK, Kwong DL, Ng SC, Tong AS, Tam EK (2012) Accuracy and sensitivity of four-dimensional dose calculation to systematic motion variability in stereotactic body radiotherapy (SBRT) for lung cancer. *J Appl Clin Med Phys, **13**: 303-317*.
16. Vinogradskiy YY, Balter P, Followill DS, Alvarez PE, White RA, Starkschall G (2009) Comparing the accuracy of four-dimensional photon dose calculations with three-dimensional calculations using moving and deforming phantoms. *Med Phys, **36**: 5000-5006*.
17. Tlusty J, Ziegert J, Ridgeway S (1999) Fundamental Comparison of the Use of Serial and Parallel Kinematics for Machines Tools. *CIRP Ann Manuf Technol, **48**: 351-356*.
18. Kurekova E, Halaj M, Omachelová M, Martišovitš I (2014) Theoretical Positioning Accuracy for Serial and Parallel Kinematic Structure. *Meas Sci Rev, **14**: 243-251*.
19. Ford EC, Mageras GS, Yorke E, Ling CC (2003) Respiration-correlated spiral CT: A method of measuring respiratory-induced anatomic motion for radiation treatment planning. *Med Phys, **30**: 88-97*.
20. Keall PJ, Starkschall G, Shukla H, Forster KM, Ortiz V, Stevens CW, Mohan R (2004) Acquiring 4D thoracic CT scans using a multislice helical method. *Phys Med Biol, **49**: 2053-2067*.
21. D'Souza WD, Kwok Y, Deyoung C, Zacharapoulos N, Pepelea M, Klahr P, Yu, CX (2005) Gated CT imaging using a free-breathing respiration signal from flow-volume spirometry. *Med Phys, **32**: 3641-3649*.
22. Fitzpatrick MJ, Starkschall G, Balter P, Antolak JA, Guerrero T, Nelson C, Mohan R (2005) A novel platform simulating irregular motion to enhance assessment of respiration-correlated radiation therapy procedures. *J Appl Clin Med Phys, **6**: 13-21*.
23. Suh Y, Yi B, Ahn S, Kim J, Lee S, Shin S, Choi E (2004) Aperture maneuver with compelled breath (AMC) for moving tumors: A feasibility study with a moving phantom. *Med Phys, **31**: 760-766*.
24. Richter A, Wilbert J, Flentje M (2011) Dosimetric evaluation of intrafractional tumor motion by means of a robot driven phantom. *Med Phys, **38**: 5280-5289*.
25. Menon G, Pudney D, Smith WS (2011) Dosimetric evalua-

[Downloaded from ijrr.com on 2026-11-24]

tion of breast radiotherapy in a dynamic phantom. *Phys Med Biol,* ***56****: 7405-7518*.

26. Court LE, Seco J, Lu X-Q, Ebe K, Mayo C, Ionascu D, Lingos T (2010) Use of a realistic breathing lung phantom to evaluate dose delivery errors. *Med Phys,* ***37****: 5850-5857*.

[Downloaded from ijrr.com on 2026-11-24]